Facile solvothermal synthesis of BiOI microsquares as a novel electrode material for supercapacitor applications

Article *in* Materials Letters · September 2017

DOI: 10.1016/j.matlet.2017.08.137

9 authors, including:

Vadivel Sethumathavan
PSG College of Technology
30 PUBLICATIONS **143** CITATIONS
SEE PROFILE

Balakrishnan Saravanakumar
Dr. Mahalingam College of Engineering and T…
14 PUBLICATIONS **235** CITATIONS
SEE PROFILE

Dr. A Manikandan
Bharath University
117 PUBLICATIONS **1,043** CITATIONS
SEE PROFILE

Ramadoss Govindarajan
PSG Institute of Advanced Studies
10 PUBLICATIONS **79** CITATIONS
SEE PROFILE

Materials Letters 210 (2018) 109–112

Contents lists available at ScienceDirect

Materials Letters

journal homepage: www.elsevier.com/locate/mlblue

Facile solvothermal synthesis of BiOI microsquares as a novel electrode material for supercapacitor applications

S. Vadivel [a,*], B. Saravanakumar [b], M. Kumaravel [a], D. Maruthamani [a], N. Balasubramanian [c], A. Manikandan [d], Govindarajan Ramadoss [e], Bappi Paul [f], S. Hariganesh [a]

[a] Department of Chemistry, PSG College of Technology, Coimbatore 641004, India
[b] Department of Physics, Dr. Mahalingam College of Engineering and Technology, Pollachi 642003, Tamil Nadu, India
[c] Electrochemical Engineering Laboratory, Department of Chemical Engineering, A.C. Tech Campus, Anna University, Chennai 600025, India
[d] Dept. of Chemistry & Central Research Laboratory, Bharath Institute of Higher Education and Research, Chennai 600073, Tamil Nadu, India
[e] PSG Institute of Advanced Studies, Coimbatore 641004, India
[f] Department of Chemistry, National Institute of Technology, Silchar 788010, Assam, India

ARTICLE INFO

Article history:
Received 29 July 2017
Received in revised form 30 August 2017
Accepted 31 August 2017
Available online 4 September 2017

Keywords:
BiOI
Semiconductors
Supercapacitors
Interfaces

ABSTRACT

BiOI microsquares was prepared by using hexamine as surfactant through solvothermal approach and used as electrode material for high performance supercapacitor. The crystalline structure and morphology of the BiOI were characterized by X-ray diffraction (XRD), field emission scanning electron microscopy (FE-SEM) transmission electron microscopy (TEM) and X-ray photoelectron spectroscopy (XPS) analysis. The electrochemical performance was investigated by using cyclic voltametry (CV) and galvanostatic charge-discharge studies (GCD) using 6M KOH solutions. BiOI electrode exhibits highest specific capacitance of 706 Fg^{-1} at a current density of 2 Ag^{-1}. This material retained 55% initial capacitance at a higher current density of 10 Ag^{-1} indicating its better rate performance.

1. Introduction

The growing demands for portable electrochemical energy storage devices have been provoked on past few decades [1]. Among the different kinds of electrochemical energy storage devices supercapacitors have attracted tremendous attention all over the world owing to their high power density, fast charge-discharge capability, and long service life [2]. Based on their energy storage property, supercapacitors can be classified into electrical double-layer capacitor (EDLC) and pseudocapacitor [3]. Due to the fast and reversible redox properties, pseudocapacitor electrode materials possess superior energy density and specific capacitance when compared to EDLC type [4]. In general, high conductivity, good redox reversibility, environment compatibility is the characteristics of a better pseudocapacitive electrode material. Generally, various forms of ruthenium based electrodes exhibits excellent capability to provide higher specific capacitance, but high cost and toxicity makes it unsuitable for commercialization [5]. Therefore, searching for a low cost pseudocapacitor material has been the prime focus in the supercapacitor research. Recent literatures revealing that bismuth based materials could be used in several energy storage devices including supercapacitors and lithium ion batteries due to their fast reversible redox properties [6]. In this context, recently our group reported various bismuth based materials like Bi_2S_3 [4], Bi_2O_3 [5] and $BiPO_4$ [6] for supercapacitor applications. In this present work, BiOI is utilized as a pseudocapacitor electrode for the first time. According to the previous literatures, it was proven that BiOI serves as an efficient material for antimicrobial agent and photocatalysts only [7] etc. However to the best of our knowledge there is no report for BiOI employed as supercapacitor electrode material.

2. Experimental detail

2.1. Material synthesis

In a typical solvothermal synthesis of BiOI, 1 mmol of $Bi(NO_3)_3 \cdot 5H_2O$ and 0.5 mmol of hexamine were dissolved in 30 mL of ethylene glycol under magnetic stirring. Afterward, 10 mL of KI solution (1 mmol of KI dissolved in water) was added drop wise into the previous solution. The above mixture was transferred into a 100 mL Teflon-lined autoclave and placed in furnace at 140 °C for 16 h and then cooled to room temperature naturally. After cooling

* Corresponding author.
E-mail address: vlvelu7@gmail.com (S. Vadivel).

http://dx.doi.org/10.1016/j.matlet.2017.08.137
0167-577X/

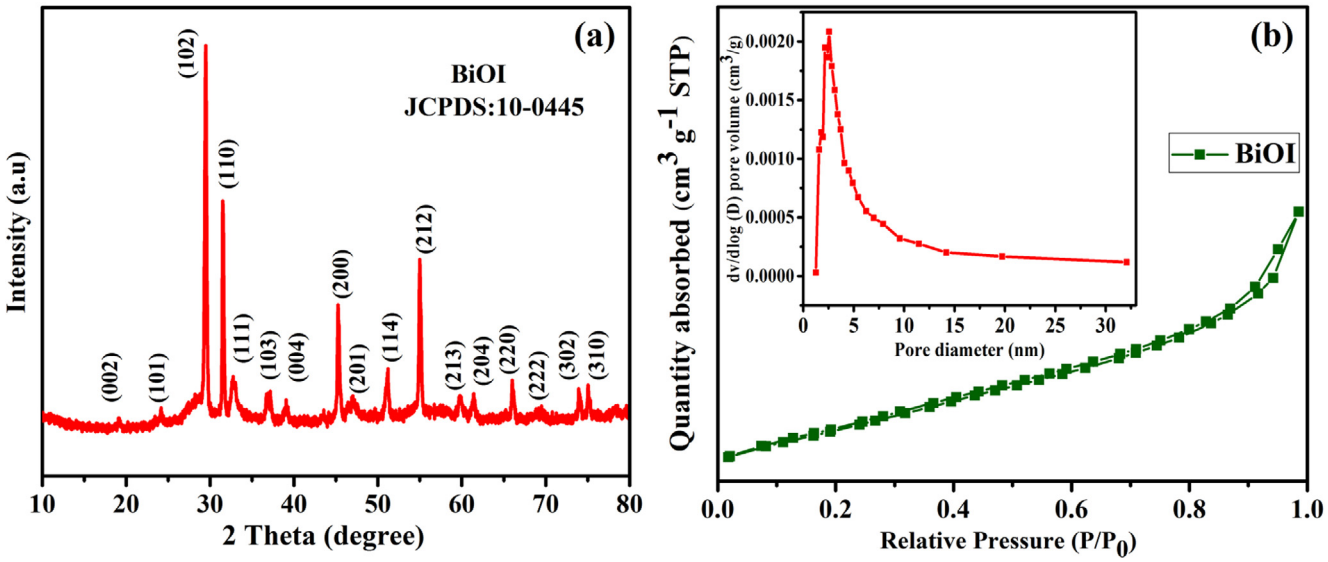

Fig. 1. (a) XRD patterns of the BiOI (b) N2 adsorption isotherm and the corresponding pore size distribution (inset) of BiOI.

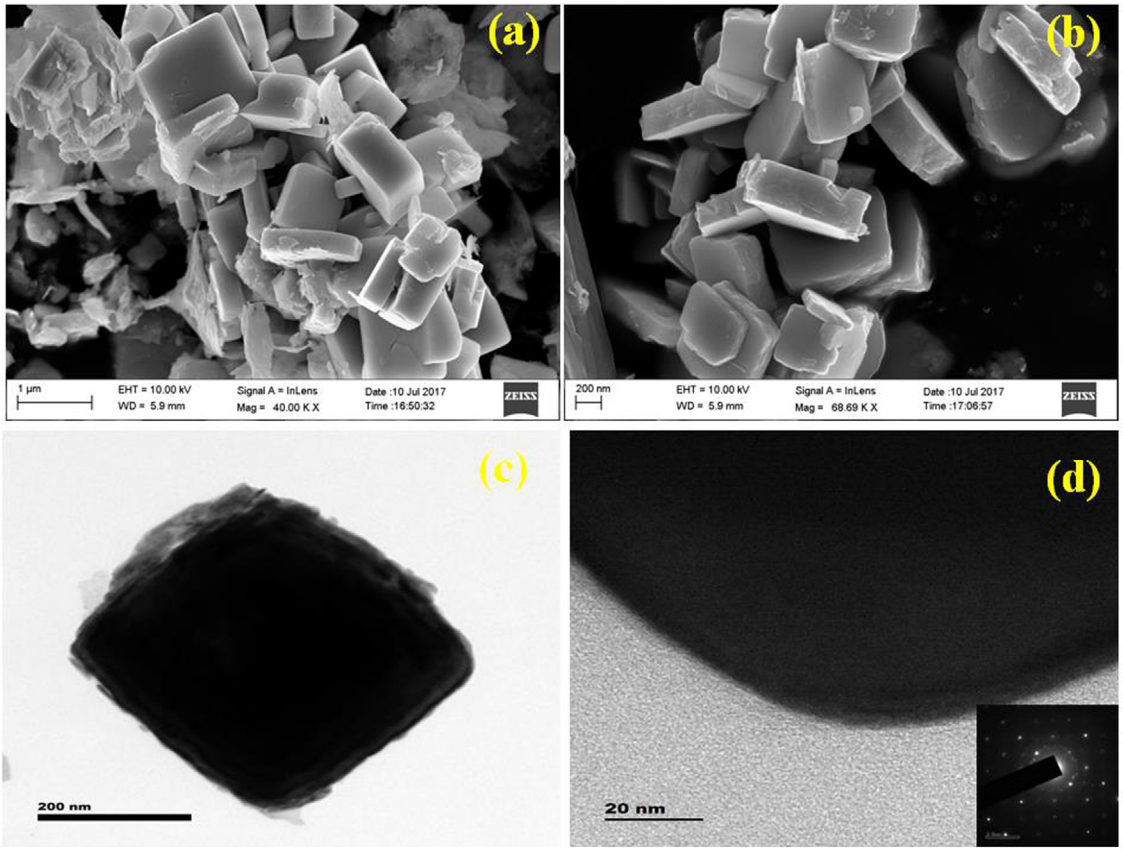

Fig. 2. (a, b) FESEM images of BiOI at different magnifications (c, d) TEM images of BiOI and the corresponding SAED pattern (inset) of BiOI.

the resultant product was washed several times with acetone, and dried at 60 °C overnight.

2.2. Material characterizations and electrochemical measurements

The XRD pattern of the BiOI sample was recorded using X-Pert Pro Pan analytical X-ray diffractometer. TEM analysis was performed on a JEOL JEM 2100.microscope. FESEM images were taken with a Zeiss EVO18 electron microscope. The N_2 adsorption-desorption studies were measured by using a Quanta chrome ASiQ win instrument. The XPS was analyzed by Ms. Omicron 1000 X-ray photoelectron spectrometer. The working electrode was prepared by mixing of 75 wt% BiOI 15 wt% of carbon black and 10 wt% of polytetrafluoroethylene (PTFE). The mixture was homogenously mixed by few drops of ethanol and the resulting mixture was coated uniformly into the stainless steel electrode and dried at

60 °C. All the electrochemical experiments were carried out using a standard three electrode system using CHI660D electrochemical workstation using 6M KOH as electrolyte. The specific capacitance (Fg^{-1}) values were obtained by using following relation [6].

$$\text{Specific capacitance} = \frac{I \times \Delta t}{m \times \Delta V}\ Fg^{-1} \quad (1)$$

where I (A) is the current density, Δt (s) is the discharge time, Δv is the potential window and m (g) is the mass of the electrode active material (1 mg).

3. Results and discussion

The phase purity and structure of the BiOI was confirmed by XRD analysis. Fig. 1(a) shows that all the diffraction peaks are well indexed to the (0 0 2), (1 0 1), (1 0 2), (1 1 0), (1 1 1), (1 0 3), (0 0 4), (2 0 0), (2 0 1), (1 1 4), (2 1 2), (2 1 3), (2 0 4), (2 2 0), (2 2 2), (3 0 2), (3 1 0) planes of the standard data for BiOI (JCPDS card no: 10-0445) which confirms the formation of the tetragonal BiOI structure [8]. The N_2 adsorption-desorption isotherms of the BiOI (Fig. 1b) reveals a type IV isotherm, representing the mesoporous characteristics of the synthesized materials. The BiOI microsquares exhibits the surface area of 32.5 $m^2\ g^{-1}$ with average pore size of 3.5 nm (mesoporous type), which are beneficial to enhance the electrochemical performance of the BiOI because they can provide more diffusion pathways for the ion transport, and offers more active sites for the interaction between electrode and electrolyte [9].

The surface morphology of the synthesized BiOI microsquares was analyzed using FE-SEM and TEM analysis. The FE-SEM images of BiOI microsquares synthesized using hexamine as stabilizing agent was represented in Fig. 2(a, b). The BiOI sample was comprised of uneven square shaped structure with average length of 2.5–4 μm. The average edge thickness of BiOI is 1 μm respectively. To obtain more structural information about the synthesized samples, TEM analysis was carried out. Much similar to FE-SEM images, the square shaped morphology was quite maintained (Fig. 2c, d) during the ultrasonication process for sample preparation for TEM analysis. The SAED patterns of the BiOI micro square sample (inset Fig. 2d) confirms the polycrystalline nature and the corresponding ring type exemplifies the BiOI crystals were oriented in different directions.

The XPS survey spectrum in (Fig. 3a) indicating that no peaks of elements other than Bi, O and I in the sample, a proof of the high purity of the BiOI microsquares. The peaks observed at 159.2 and 164.5 eV in Fig. 3(b) ascribed to the Bi 4f $_{7/2}$ and Bi 4f $_{5/2}$ spins which confirms the oxidation state of bismuth in the sample is Bi^{3+}. The two broad peaks centered at 619.1 and 630.9 eV are ascribed to I $3d_{5/2}$ and I $3d_{3/2}$ spin (Fig. 3c) indicating the oxidation state of I is −1. The O1s spectrum shows the prominent peal at 530.5 eV (Fig. 3d) which is originated from the lattice oxygen of metallic oxide (Bi-O) [10].

Electrochemical performances of BiOI microsquares were evaluated at different scan rate between the potential window −1.0 and 0 V using three electrode system. The distinct redox peaks observed from CV curves in Fig. 4a reveals that the capacitive behavior of the BiOI is due to the oxidation/reduction reactions of Bi and Bi^{3+} which is pseudo capacitive in nature. The redox peaks at −0.49 V and −0.83 V for the BiOI is mainly due to the redox reactions of metallic bismuth into Bi^{3+}. The small peak around -0.61 V is due to the oxidation of untransformed Bi form BiOI matrix [11]. The shape of CV curves are maintained even at high scan rates which further confirms the better pseudo capacitive behavior and the fast diffusion of ions into the BiOI. The CV curves are quite consistent with previous report by Tong et al. [12] Fig. 4(b) indicates the non-linear galvanostatic charge-discharge curves which shows the ideal pseudocapacitive behavior of BiOI and agrees quietly with the CV studies. The specific capacitance values are determined using the equation (1) are 706, 448, 408, 396, 389 Fg^{-1} (Fig. 4c) at 2, 4, 6, 8, 10 Ag^{-1} respectively. As presented from Fig. 4(c) the specific capacitance value decreases with increase in current density is due to insufficient access time for electrolyte

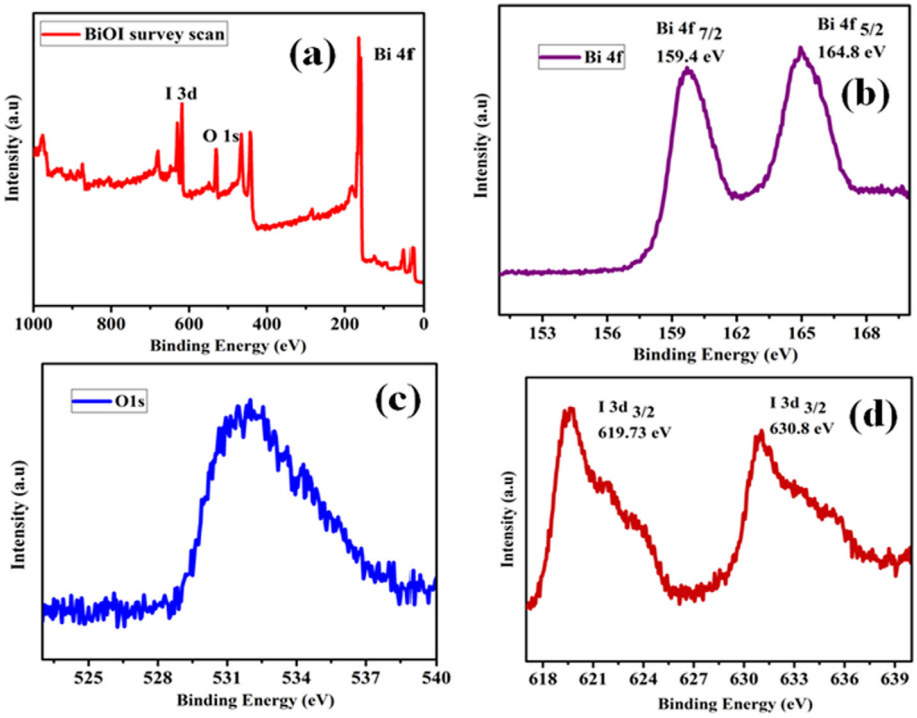

Fig. 3. (a) XPS survey spectrum of BiOI and high-resolution XPS of (b) Bi4f, (c) O1s and (d) I 3d.

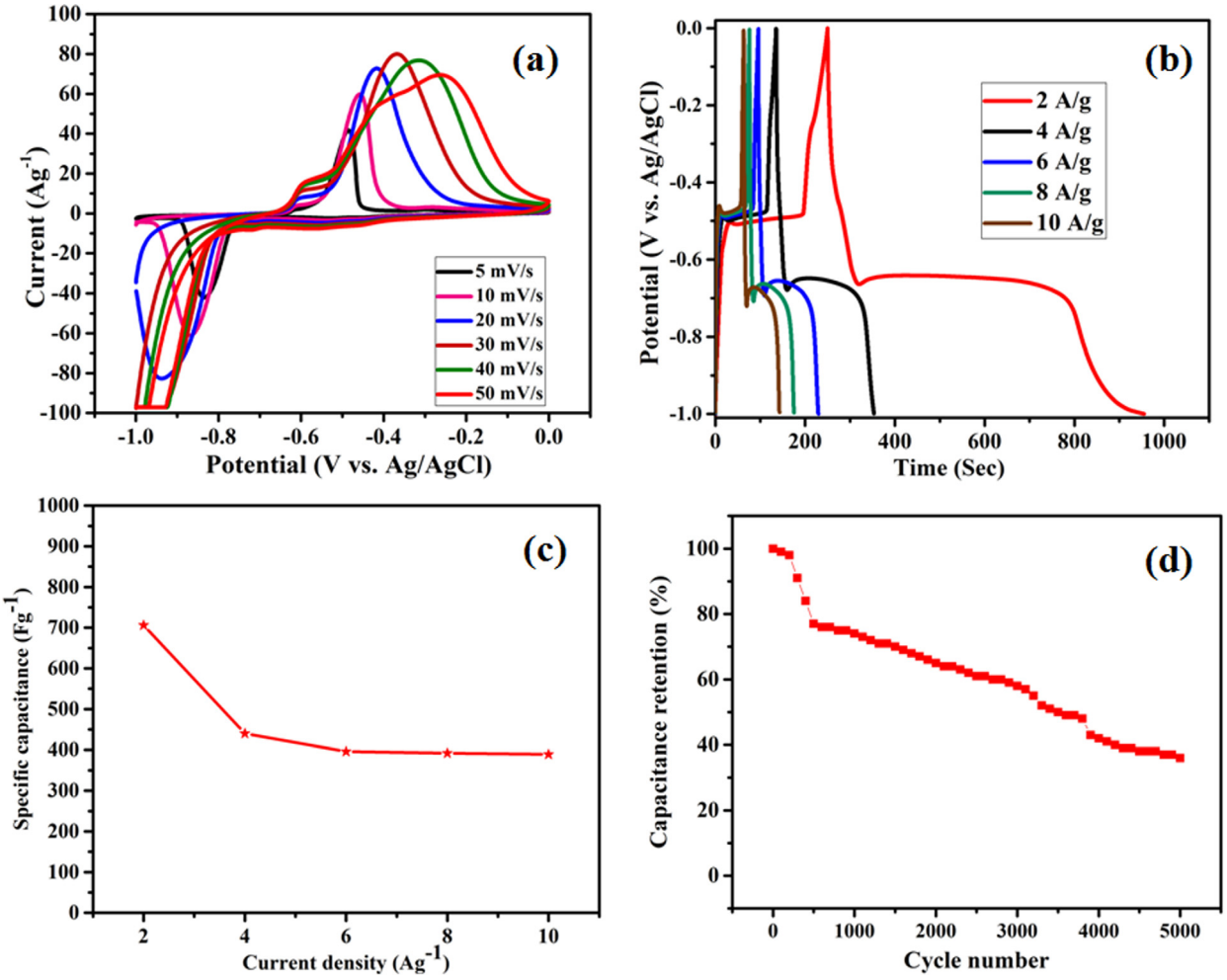

Fig. 4. (a) Electrochemical performance of BiOI (a) CV curves at a different scan rates (b) charge-discharge studies at a different current densities (c) Variation of specific capacitances of with respect to current density (d) Cyclic stability test for BiOI electrode.

ion into the electrode active material at higher current densities. There is nearly 55% of capacitance retention even when the current density is increased by 5 times. This BiOI electrode holds 78% of capacitance after 1000 cycles and retails 36% of after 5000 cycles (Fig. 4d) suggesting the better cyclic stability. This fading of capacitance is due to the volumetric stress produced due to ion intercalation during cycling process [13]. This volumetric change is confirmed by SEM, XRD and XPS measurements after 5000 cycles Figs. (S1–S4).

4. Conclusion

In summary, BiOI microsquares have been synthesized by solvothermal approach using hexamine as surfactant. As an electrode material for supercapacitors, BiOI exhibits high specific capacitance and good rate capability due to high surface area and superior redox behavior of the material. This present study demonstrates that the square shaped BiOI is a promising alternate electrode material for high-performance supercapacitors in near future.

Acknowledgement

This work was financially supported by DST- Science and Engineering Research Board (SERB) India, under **"Early Career Research Award Scheme" (ECR/2016/001535/CS)** to Dr.S.Vadivel.

Appendix A. Supplementary data

Supplementary data associated with this article can be found, in the online version, at http://dx.doi.org/10.1016/j.matlet.2017.08.137.

References

[1] E.J. Lee, J.H. Bang, Mater. Lett. 105 (2013) 28–33.
[2] B. Zhang, W. Li, J. Sun, G. He, R. Zou, J. Hu, Z. Chen, Mater. Lett. 114 (2014) 40–43.
[3] Y. Han, S. Zhang, Na. Shen, D. Li, X. Li, Mater. Lett. 188 (2017) 1–4.
[4] S. Vadivel, A. Nirmalesh Naveen, V.P. Kamalakannan, P. Cao, N. Balasubramanian, Appl. Surf. Sci. 351 (2015) 635–645.
[5] D. Maruthamani, S. Vadivel, M. Kumaravel, B. Saravanakumar, B. Paul, S.S. Dhar, A.H. Yangjeh, A. Manikandan, G. Ramadoss, J. Colloid. Interf. Sci 498 (2017) 449–459.
[6] S. Vadivel, A.N. Naveen, J. Theerthagiri, J. Madhavan, T. Santhoshini Priya, N. Balasubramanian, Ceram. Int. 42 (2016) 14196–14205.
[7] Z. Jiang, X. Liang, Y. Liu, T. Jing, Z. Wang, X. Zhang, X. Qin, Y. Dai, B. Huang, Appl. Catal. B-Environ. 211 (2017) 252–257.
[8] J. Su, Y. Xiao, M. Ren, Catal. Commun. 45 (2014) 30–33.
[9] M. Cheng, S. Duan, H. Fan, X. Su, Y. Cui, R. Wang, Chem. Eng. J. 327 (2017) 100–108.
[10] Y. Cong, Y. Ji, Y. Ge, H. Jin, Y. Zhang, Q. Wang, Chem. Eng. J. 307 (2017) 572–582.
[11] Y.C. Zhang, H. Yang, W.P. Wang, H.M. Zhang, R.S. Li, X.X. Wang, R.C. Yu, J. Alloys Compd. 684 (2016) 707–713.
[12] Y. Tong, C. Zheng, W. Lang, F. Wu, T. Wu, W. Luo, H. Chen, Mater. Des. 122 (2017) 90–101.
[13] D. Guo, Y. Luo, X. Yu, Q. Li, T. Wang, Nano Energy 8 (2014) 174–182, 1686.

INTERNATIONAL JOURNAL OF HYDROGEN ENERGY 42 (2017) 28445–28452

Available online at www.sciencedirect.com

ScienceDirect

journal homepage: www.elsevier.com/locate/he

Hierarchical mesoporous $Co_x Ni_{1-x}O$ as advanced electrode material for hybrid supercapacitors

Kamatchi Kamaraj Purushothaman [a,*], *Inbamani Manohara Babu* [b], *Balakrishanan Saravanakumar* [c]

[a] *Research Centre, Department of Physics, SSM Institute of Engineering and Technology, Dindigul, 624002, Tamilnadu, India*

[b] *Department of Physics, Gandhigram Rural University, Gandhigram, 624302, Tamilnadu, India*

[c] *Faculty of Physics, Mahalingam College of Engineering and Technology, Pollachi, Tamil Nadu, India*

ARTICLE INFO

Article history:
Received 24 May 2017
Received in revised form
25 July 2017
Accepted 21 September 2017
Available online 16 October 2017

Keywords:
Nanosheets
Porous networks
Supercapacitor
Nickel oxide
Hydrothermal

ABSTRACT

The nanosheets interconnected highly porous $Co_xNi_{1-x}O$ ($0.025 \leq x \leq 0.1$) was successfully synthesized via hydrothermal route. The effect of Co on the structural, morphological and electrochemical properties of NiO has been examined for supercapacitor (SC) application. Scanning electron microscope (SEM) images display the formation of porous networks. Scanning transmission electron microscope (STEM) images confirm the arrangement of nanosheets leads to flower like porous networks. $Co_{0.05}Ni_{0.95}O$ exhibits the maximum specific capacity of 582 C g^{-1} (161.67 mA h g^{-1}) at a specific current of 1 A g^{-1}. Galvanostatic charge discharge (GCD) analysis reveals the maximum energy density of 39.54 W h kg^{-1} with the power density of 17.11 kW kg^{-1}, and observed cyclic stability is 96% even after 1500 continuous charge/discharge cycles for $Co_{0.05}Ni_{0.95}O$.

Introduction

Global warming, climate change and the decreasing availability of fossil fuels force the society to more concentrate about sustainable and renewable resources. As a result, we are giving greater attention to renewable energy production ie. Energy from sun, wind etc …, as well as the development of electric vehicles or hybrid electric vehicles with low CO_2 emission. The sun does not shine during the night and wind does not blow on demand, this situation leads to think about advanced energy storage systems such as batteries and electrochemical capacitors (ECs) [1]. ECs, have been considered as one of the most promising candidates as energy storage system due to its special features like higher power density, faster charge–discharge process and longer lifespan compared to batteries [2,3]. Intensive research works have been dedicated around the globe to investigate the possible electrode materials such as hydroxides [4,5], metal oxides [6–8] and polymers [9,10]. Among different kinds of transition metal oxides, ruthenium dioxide (RuO_2) has been considered as a most promising electrode material because of its multiple redox states and good electrical conductivity [11,12]. The high cost and toxic nature of this noble material restricts its use in commercial supercapacitors [1].

The battery type Faradaic electrode materials (nickel oxide, cobalt oxide) are attract the attention of researchers due to its

* *Corresponding author.*
E-mail address: purushoth_gri@yahoo.co.in (K.K. Purushothaman).
https://doi.org/10.1016/j.ijhydene.2017.09.115

importance in hybrid supercapacitors or supercapattery (supercapacitor + battery) applications [13–16]. NiO has been widely investigated as electrode material for energy storage applications like lithium-ion batteries and supercapacitors due to its high theoretical capacity of 290 mA h g^{-1} for one electron reaction in alkaline electrolyte [16–23]. In order to enhance the energy storage capacity and cyclic stability much more efforts has been devoted to the controlled synthesis of various NiO nanostructures [24–28]. Despite the great progress, the capacity is still far below to its theoretical value and the cyclic stability is also not very much satisfactory. To overcome this issue some of the foreign element may added with NiO. Tang et al [29] studied the charge storage behavior of hierarchically porous Ni–Co oxide. Zheng et al [30] prepared the cobalt doped NiO hexagonal nanoplatelets for energy storage applications. NiO/graphene composite has been prepared and analyzed for possible hybrid supercapacitor applications [31–33]. Herein we report a simple and cost effective route to fabricate Co doped NiO nanostructures. The effect of Co on the structural, morphological and electrochemical properties of NiO has been studied and discussed.

Experimental section

Synthesis of Co doped NiO

Analytical grade Nickel nitrate, Cobalt nitrate, SDS (sodium lauryl sulphate) and urea were purchased and used without further purification. In the typical synthesis process 0.1081 g of SDS was dispersed in 50 ml double distilled (DD) water and stirred continuously for 30 min. 0.4253 g of $Ni(NO_3)_2.6H_2O$ and 0.0104 g of $Co(NO_3)_2.6H_2O$ (corresponds to 2.5 wt % of Co) was dissolved in 15 ml of DD water. 0.1801g of urea was dissolved in 10 ml separately. The two solutions were added slowly to SDS solution. The resultant solution was stirred at room temperature for 3 h and finally transferred to a 100 mL Teflon lined stainless steel autoclave. The autoclave was kept at 160 °C for 24 h and finally allowed to cool at room temperature. A solid green product was obtained by centrifugation. This product was repeatedly washed with ethanol and double distilled water. $Co_xNi_{1-x}O$ has been obtained by annealing the green powder at 300 °C for 2 h in an atmosphere of air. The wt % of nickel nitrate and cobalt nitrate has been varied to prepare 2.5 wt%, 5.0 wt %, 7.5 wt % and 10.0 wt % of Co doped NiO. The products were finally named as CDN1, CDN2, CDN3 and CDN4 respectively. For example CDN1 would correspond to the 2.5 wt % of Cobalt doped NiO.

Material characterization

The morphological studies and elemental analysis of the samples were made using scanning electron microscope with Energy dispersive X-ray spectrometer (EDS). (SEM, JSM-6390-JEOL) and scanning transmission electron microscopy (STEM, FE-QUANTA). X-ray diffraction (XRD) patterns were recorded using PANAlytical XPERT- PRO x-ray diffractometer with CuKα radiation. Brunauer–Emmett–Teller (BET) analysis and pore size distribution was obtained from the desorption plot by Barrett–Joyner–Halenda (BJH) method using Micromeritics (ASAP 2020 V3.00 H) system.

Electrochemical testing

The working electrode has been prepared as follows. Typically, the electroactive material, Activated Carbon, and poly(tetrafluoroethylene) (PTFE) were mixed in a mass ratio of 85.0:10.0:5.0 (total mass is 1 mg) with few drops of ethanol to form homogeneous slurry. Then the slurry was coated onto nickel foam (area of 1 cm^2) and dried at 80 °C for 8 h. For electrochemical testing, a beaker-type three-electrode cell was fabricated using the Co doped NiO coated on Ni foam as working electrode, platinum wire as counter electrode, Ag/AgCl as the reference electrode and 2 M aqueous KOH solution as an electrolyte. Cyclic Voltammetry (CV), Galvanostatic Charge-Discharge (GCD) and Electrochemical Impedance Spectroscopy (EIS) measurements were carried out using Electrochemical Workstation (CHI 660D, USA). The cyclic voltammetric analysis was performed for different scan rates in the potential range of 0–0.55 V. The galvanostatic charge discharge measurements were carried out in the potential range of −0.15 V to 0.4 V for different current densities. EIS measurements were made between 0.01 Hz and 100 kHz with the amplitude of 5 mV.

Results and discussion

Structural and morphological studies

The crystal structure, phase and purity of the samples have been analyzed using powder X-ray diffraction (XRD) measurement. Fig. 1 shows the XRD patterns of Co doped NiO nanostructures, which exhibits a predominant well crystalline phase and consistent with the peak positions in the literature [34–38]. All the samples shows three significant diffraction peaks at 37.2°, 43.4° and 62.9°, which is attributed to the (111) (200) and (220) reflections of NiO with cubic structure and the planes coincide with the standard NiO patterns (JCPDS 78-0643). The same type of result was reported by Xiao [39] et al. for $Co_xNi_{1-x}O$ nanorods synthesized via Bio inspired method.

The morphological information of $Co_xNi_{1-x}O$ was revealed from SEM and STEM analysis (Fig. 2). Initially the nanosheets are formed due to the presence of an anionic surfactant [40]. The Co doping leads to the formation of flower like

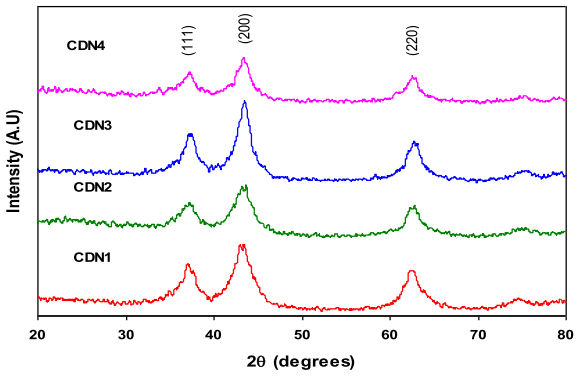

Fig. 1 – XRD patterns of CDN1, CDN2, CDN3 and CDN4.

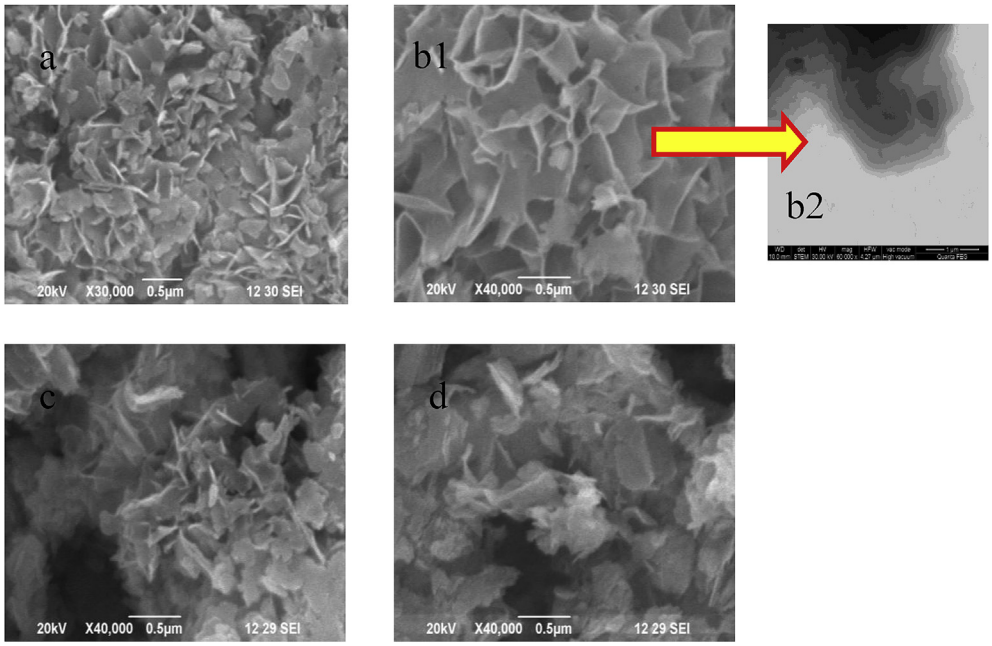

Fig. 2 – SEM images of (a) CDN1, (b1) CDN2, (c) CDN3 (d) CDN4 and STEM image of CDN2 (b2).

nanosheets interconnected porous structure upto 5 wt % of Co doping (Fig. S1.), further increase in the Co doping level leads to breaking of flower like structure and the formation of individual nanosheets. STEM image (Fig. 2 b2) confirms that the nanosheets are the basic building blocks for the interconnected network structure. Energy Dispersive X-ray Spectroscopy analysis was employed to determine the elemental composition in the samples. Fig. 3 shows the EDS spectra and the composition of elements present in the CDN1, CDN2, CDN3 and CDN4.

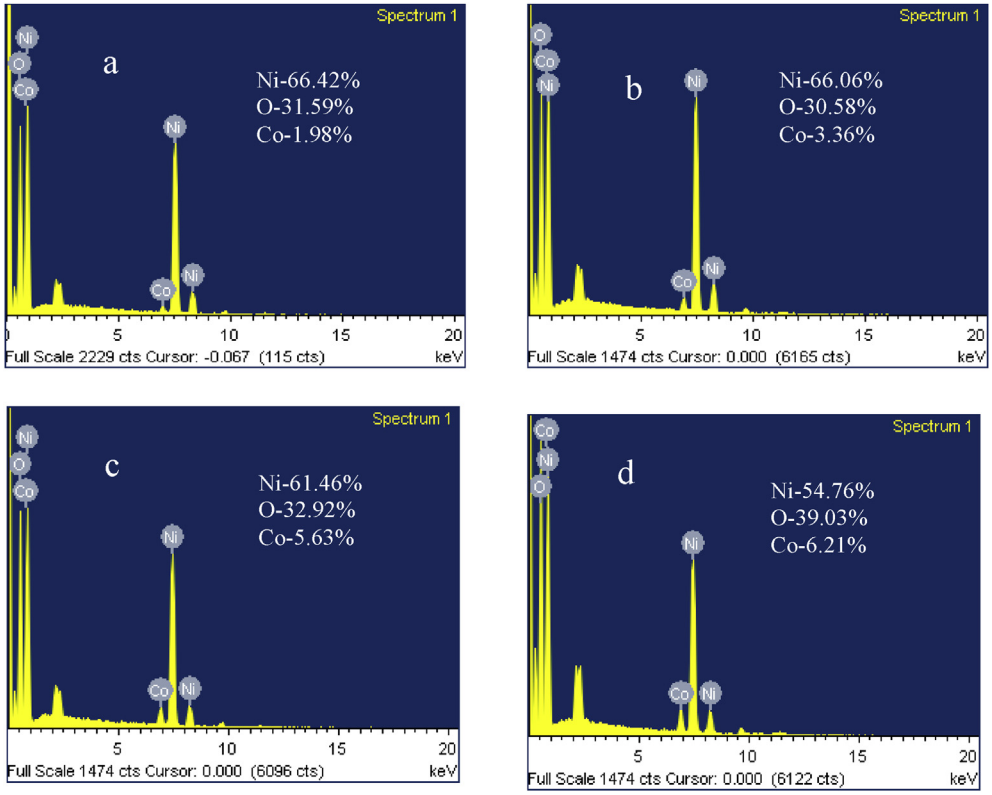

Fig. 3 – EDS patterns of (a) CDN1, (b) CDN2, (c) CDN3 and (d) CDN4.

Electrochemical behavior

To explore the potential application of the $Co_xNi_{1-x}O$, the samples were characterized by CV, GCD and EIS measurements. Fig. 4 shows the CV curves of CDN1, CDN2, CDN3 and CDN4 at different scan rates in the potential range of 0–0.55 V. The cyclic voltammogram shows well resolved redox peaks, which confirms the specific capacity arises due to surface redox reaction and not governed by pure electric double layer capacitance. Further, with an increase of the scan rate from 3 to 20 mV s^{-1}, the anodic and cathodic peaks are shifted towards higher and lower potentials respectively. This is mainly due to the limitations of the ion diffusion rate to satisfy electronic neutralization during the redox reaction.

The sample CDN2 exhibits the pre-dominant cyclic behavior due to the interconnected nanosheets network with excellent porosity [41]. The porous network provides excellent paths for mobilization of ions. Surface area is one of the key factors for the electroactive materials in supercapacitor applications. The specific surface area and porous nature of the CDN2 was investigated by nitrogen adsorption/desorption study (Fig. S2). The nitrogen adsorption isotherm of CDN2 shows type IV isotherms with H3-type hysteresis loop ($p/p_o > 0.4$), which confirms the presence of mesopores [42] with the specific surface area of 130.44 m^2 g^{-1}. The pore size distribution of CDN2 is shown in Fig. S2 (inset). The CDN2 exhibits mesoporous nature with a broad peak in the range of 2.4–28.1 nm. This may facilitate the ion movements and enhances the energy storage behavior of CDN2. At lower scan rates, the ions utilizes both inner and outer surface of the active material, which leads to increase in charge storage capacity, while at higher scan rates the ions are accessed only by outer surface [43]. Schematic representation of ion insertion and deinsertion process takes place in the nanosheets assembled porous structure is shown in Fig. 5.

GCD measurements were carried out at different current densities within the potential window of −0.15 to 0.4 V to estimate the specific capacity, energy density, power density and cyclic stability. Fig. 6 shows the GCD curves of CDN1, CDN2, CDN3 and CDN4. The specific capacity (C_g) [44] was calculated using

$$C_g = \frac{I \times \Delta t}{m \times 3.6} \quad (\mathrm{C\ g^{-1}})$$

Where I (A) is the discharge current, Δt (s) is the discharge time and m (g) is the mass of the active material (working

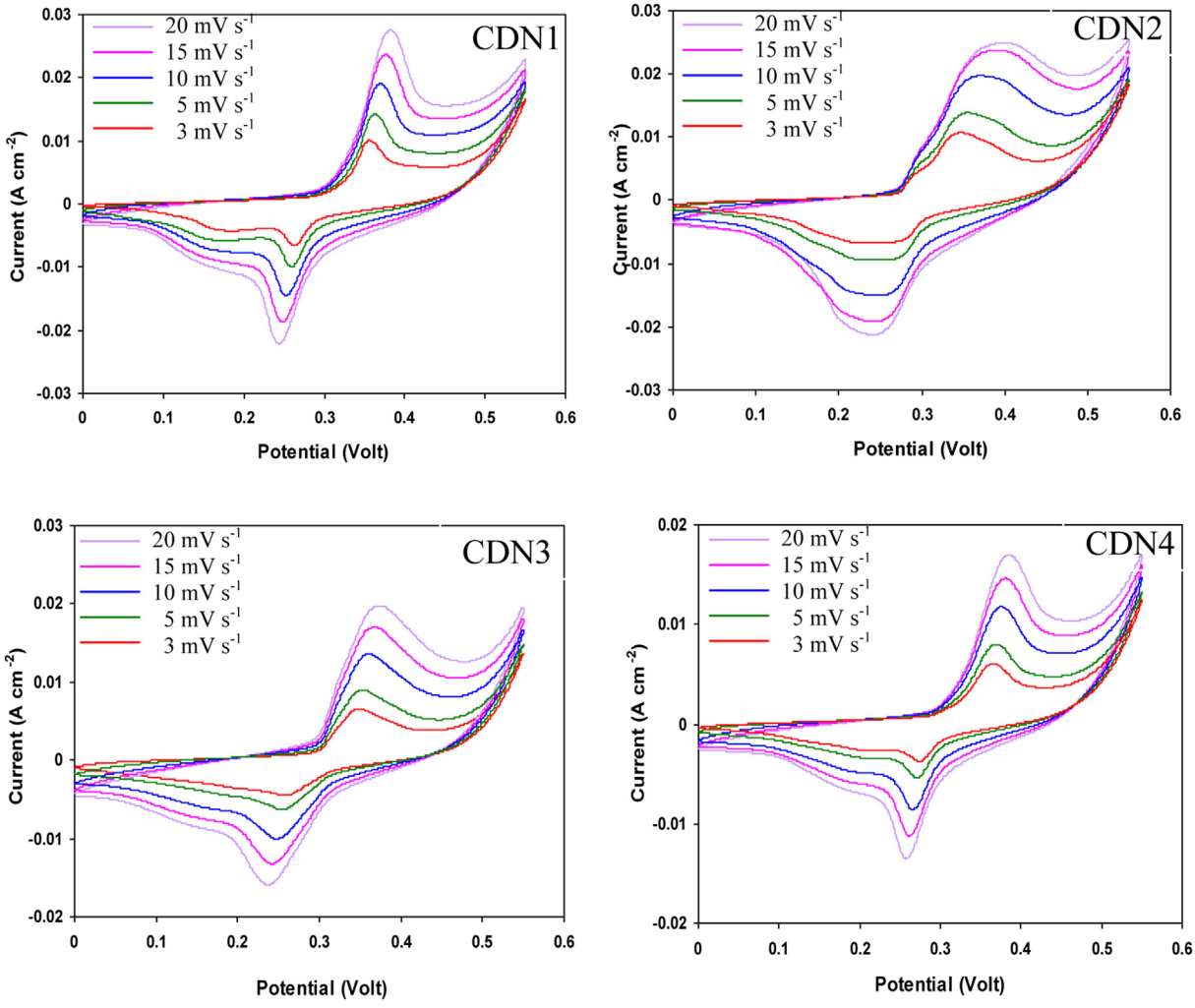

Fig. 4 – Cyclic Voltammograms of CND1, CDN2, CDN3 and CDN4 at different scan rates.

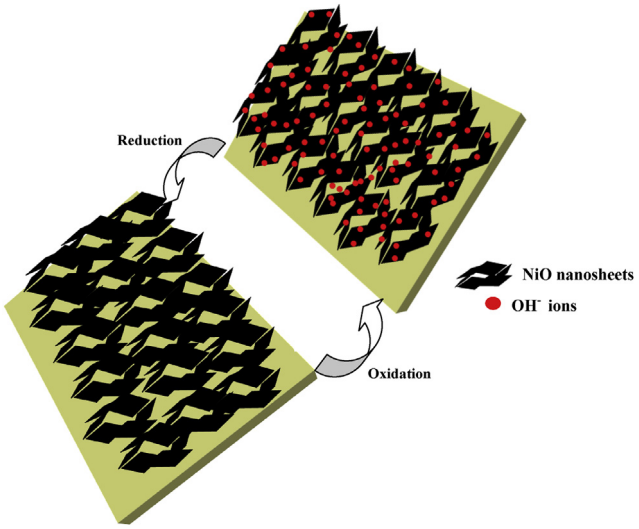

Fig. 5 – Schematic illustration of ion insertion/deinsertion.

electrode). The calculated C_g values for the samples CDN1, CDN2, CDN3 and CDN4 are 531 C g^{-1} (147.5 mA h g^{-1}), 582 C g^{-1} (161.67 mA h g^{-1}), 482 C g^{-1} (133.89 mA h g^{-1}) and 400 C g^{-1} (111.11 mA h g^{-1}) at 1 A g^{-1} respectively. Among these samples CDN2 shows higher specific capacity compared to other electrodes. Niu et al [45] reported the specific capacity of ~212 C g^{-1} (530 F g^{-1}) for NiO/C at a current density of 1 A g^{-1}. The specific capacity of ~412 C g^{-1} (909 F g^{-1}) at a current density of 1 A g^{-1} was reported by Xiao et al [39] for $Co_xNi_{1-x}O$ nanocomposites prepared via hydrothermal route. Li et al [46] reported the maximum specific capacity of ~248 C g^{-1} for nickel oxide/manganese dioxide core-shell nanosheet arrays. NiO nanoflake coated CuO flower core–shell nanostructures revealed the maximum specific capacity of 112 C g^{-1} [47]. CDN2 shows enhanced specific capacity while comparing with other works. This high capacity is attributed due to the facile interconnected nanosheets with excellent porosity, which provides better paths for electrolyte ion access. Fig. S3. Shows the plot of specific capacity as a function of current density. The increase in current density results in higher IR drop, which leads to fading of specific capacity in hierarchically interconnected CDN2.

Energy density and power density are the crucial factors, which decide the commercial usage of the electrode material. The energy density and the power density were calculated using the following equations [44]:

$$E_{int/D} = I \int_{t(V\ max)}^{t(V\ min)} V(t)dt \quad (W\ h\ kg^{-1})$$

$$E_{S,int/D} = \frac{E_{int/D}}{m3.6}$$

$$P_{max} = \frac{V^2}{4ESR} \quad (W\ kg^{-1})$$

Where $E_{int/D}$ is the discharge energy density, $E_{S,int/D}$ is the specific energy density, m is the mass of electrodes, ESR is the equivalent series resistance, V is the potential, P_{max} is the maximum power density and I is the specific current. CDN1, CDN2, CDN3 and CDN4 exhibits the specific energy density of 35.76, 39.54, 33.57 and 28.58 W h kg^{-1} with the power density of 11.55, 17.11, 11.49 and 9.53 kW kg^{-1} at the current density of 1 A g^{-1} respectively. CDN2 exhibits maximum specific energy density, which is in the range of metal hydride batteries [48].

Cyclic performance is an important characteristic of an electrochemical capacitor for practical applications. The cyclic stability of the CDN2 was evaluated by continuous charge/discharge cycles between −0.15 to 0.4 V at a current density of 5 A g^{-1} (Fig. 7). CDN2 electrode shows 96% capacity retention after 1500 cycles. Wang et al. [49] reported 8% loss after 500

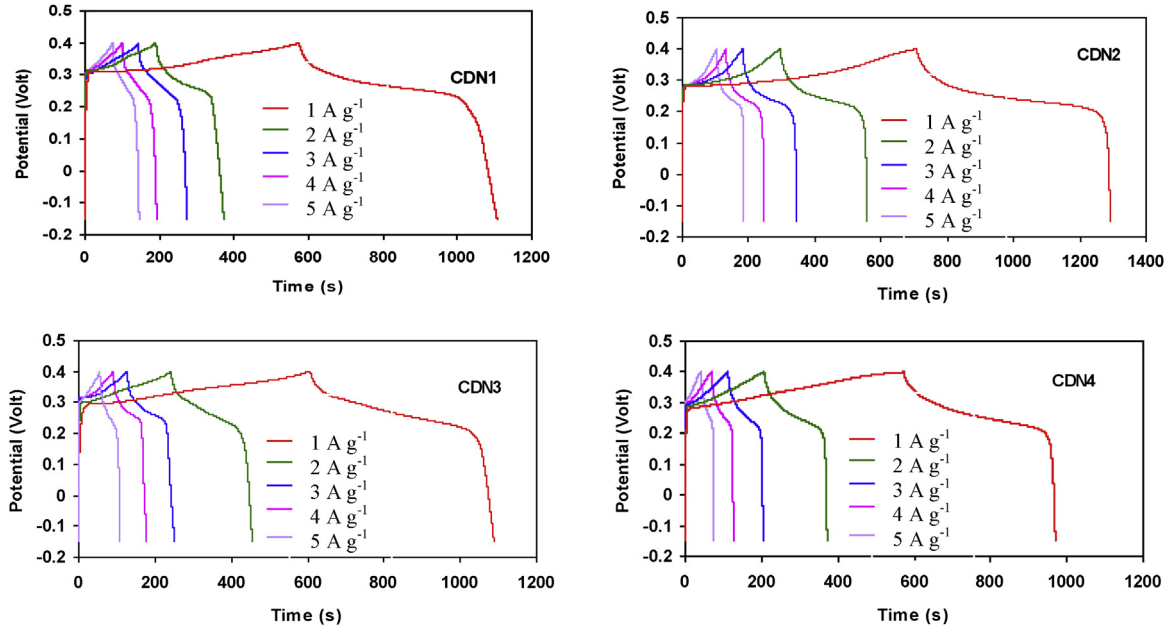

Fig. 6 – Charge/discharge curves of CDN1, CDN2, CDN3 and CDN4 samples at different current densities.

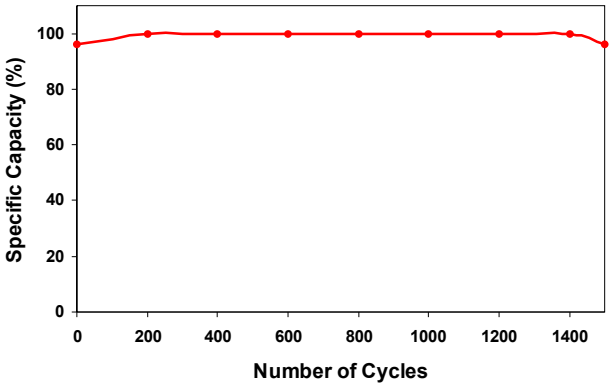

Fig. 7 – Cyclic performance of CDN2 at constant current density of 5 A g^{-1}

continuous charge/discharge cycles at a current density of 2 A g^{-1} for Co_x Ni_y O nanostructures. MnO_2–NiO hybrid nanoarrays exhibit 3.6% loss after 1500 continuous charge/discharge cycles [50]. These reports suggest that CDN2 is a permissible electrode material for hybrid supercapacitors with excellent cyclic stability.

Electrochemical impedance spectroscopy is an important method to analyze the electrochemical performance of the electrodes. Fig. 8a shows the Nyquist plot. The Nyquist plot for CDN1, CDN2, CDN3 and CDN4 was recorded in the frequency range of 0.01 Hz–100 kHz at a potential of 0.4 V. The impedance spectra comprised of one semicircle at high-frequency region (inset of Fig. 8a) and the straight line at low-frequency region. The modified Randles circuit is shown in Fig. 8b where the R_s stands for solution resistance of the electrochemical system and internal resistance of the electrode materials, R_{ct} denotes Faradic charge transfer resistance, C_L & C_{DL} denotes the ideal polarizable capacitance and the double layer capacitance, R_L denotes the leakage resistance. The slope of 45° portion of the curve is due to the Warburg resistance. The solution resistance of the CDN1, CDN2, CDN3 and CDN4 are 6.08, 5.53, 5.82 and 6.05 Ω respectively, while the R_{ct} values are 6.56, 4.42, 6.58 and 7.93 Ω respectively.

The Faradaic charge transfer resistance is a well-known limiting factor of specific capacity [51]. CDN2 exhibits lower charge transfer resistance and it facilitates the transportation of ions during electrochemical reactions. Improved ion transport and the depressed polarization may be attributed due to the substantial decrease in charge transfer resistance

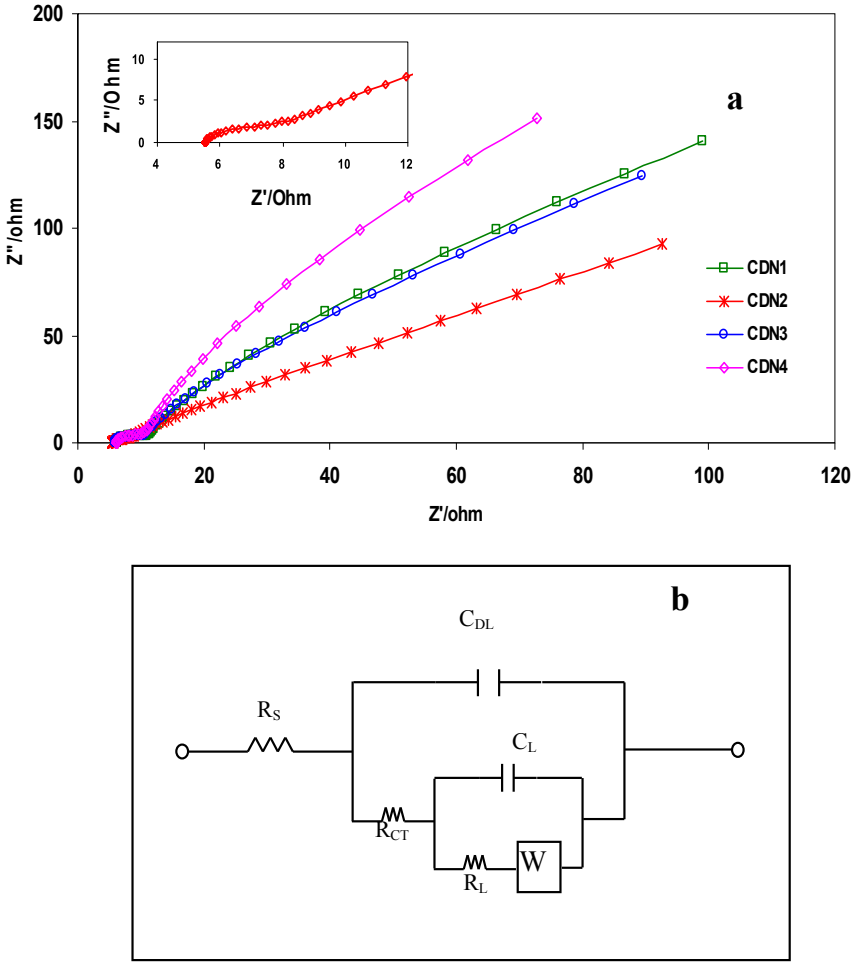

Fig. 8 – (a).Nyquist plot of CDN1, CDN2, CDN3 and CDN4 samples at 0.4 V; inset shows the high frequency region of CDN2. (b) Equivalent Randles circuit.

[52]. CDN2 electrode has notably low R_{ct}, which significantly increases the energy density and specific capacity.

Conclusion

Hierarchical Co doped NiO nanostructures have been synthesized via simple and cost effective hydrothermal method. 5 wt % of Co doped NiO exhibits the maximum specific capacity (585 C g^{-1}), energy density (39 W h kg^{-1}) & power density (17.11 kW kg^{-1}). The porous networks improve the supercapacitive performance by providing excellent paths for ions. The lower charge transfer resistance and excellent cyclic stability of 5 wt % of Co doped NiO shows its ability to serve as a potential candidate for hybrid supercapacitor applications.

Acknowledgement

One of the authors (K.K.P.) thanks Department of Science and Technology-, New Delhi, India, for providing the financial support under Young Scientist scheme (Sanction No: SR/FTP/PS-030/2011) and Nanotechnology Research Centre, SRM University, Kattankulathur, India, for providing XRD and STEM facility.

Appendix A. Supplementary data

Supplementary data related to this article can be found at https://doi.org/10.1016/j.ijhydene.2017.09.115.

REFERENCES

[1] Simon P, Gogotsi Y. Materials for electrochemical capacitors. Nat Mater 2008;7:845–54.
[2] Miller JR, Simon P. Electrochemical capacitors for energy management. Science 2008;321:651–2.
[3] Wang GP, Zhang L, Zhang J. A review of electrode materials for electrochemical supercapacitors. J Chem Soc Rev 2012;41:797–828.
[4] Yuan YF, Xia XH, Wu JB, Yang JL, Chen YB, Guo SY. Nickel foam- supported porous Ni(OH)/NiOOH composite film as advanced pseudocapacitor material. Electrochim Acta 2011;56:2627–32.
[5] Liu CG, Lee YS, Kim YJ, Song IC, Kim JH. Electrochemical characteristics of hydrothermally deposited nickel hydroxide on multi-walled carbon nanotube for supercapacitor electrode. Synth Met 2009;159:2009–12.
[6] Wu JB, Lin Y, Xia XH, Xu JY, Shi QY. Pseudocapacitive properties of electrodeposited porous nanowall Co_3O_4 film. Electrochim Acta 2011;56:7163–70.
[7] Wu JB, Li ZG, Lin Y. Porous NiO/Ag composite film for electrochemical capacitor application. Electrochim Acta 2011;56:2116–21.
[8] Kim JH, Choi HJ, Kim HK, Lee SH, Lee YH. A hybrid supercapacitor fabricated with an activated carbon as cathode and an urchin-like TiO_2 as anode. Int J Hydrogen Energy 2016;41(31):13549–56.
[9] Huang JH, Chu CW. Achieving efficient poly(3,4-ethylenedioxythiophene)- based supercapacitors by controlling the polarization kinetics. Electrochim Acta 2011;56:7228–34.
[10] Guan H, Fan LZ, Zhang HC, Qu XH. Polyanniline nanofibers obtained by interfacial polymerization for high-rate supercapacitors. Electrochim Acta 2010;56:964–8.
[11] Zhang J, Ma J, Zhang LL, Guo P, Jiang J, Zhao XS. Template synthesis of tubular ruthenium oxide for supercapacitor applications. J Phys Chem C 2010;114:13608–13.
[12] Lin Y, Zhao N, Nie W, Ji X. Synthesis of ruthenium dioxide nanoparticles by a two-phase route and their electrochemical properties. J Phys Chem C 2008;112:16219–24.
[13] Wang X, Li M, Chang Z, Wang Y, Chen B, Zhang L. Orientated Co_3O_4 nanocrystals on MWCNTs as superior battery-type positive electrode material for a hybrid capacitor. J Electrochem Soc 2015;162:A1966–71.
[14] Zhou Q, Wang X, Liu Y, He Y, Gao Y, Liu J. High rate capabilities of $NiCo_2O_4$-based hierarchical superstructures for rechargeable charge storage. J Electrochem Soc 2014;161:A1922–6.
[15] Yu L, Chen GZ. High energy supercapattery with an ionic liquid solution of $LiClO_4$. Faraday Discuss 2016;190:231–40.
[16] Brousse T, Belanger D, Long JW. To be or not to be pseudocapacitive? J Electrochem Soc 2015;162:A5185–9.
[17] Lu KC, Anderson MA. Porous nickel oxide/nickel films for electrochemical capacitors. J Electrochem Soc 1996;143:124–30.
[18] Wang B, Chen JS, Wang Z, Madhavi S, Lou XW. Green synthesis of NiO nanobelts with exceptional pseudocapacitive properties. Adv Energy Mater 2012;2:1188–92.
[19] Cao F, Zhang F, Deng RP, Hu W, Liu DP, Song SY, et al. Surfactant-free preparation of NiO nanoflowers and their lithium storage properties. J Cryst Eng Comm 2011;13:4903–8.
[20] Xu J, Lin F, Marca M, Tong DW. A review of Ni-based layered oxides for rechargeable Li-ion batteries. J Mater Chem A 2017;5:874–901.
[21] Wang XH, Li XW, Sun XL, Li F, Liu QM, Wang Q, et al. Nanostructured NiO electrode for high rate Li-ion batteries. J Mater Chem 2011;21:3571–3.
[22] Xiong SL, Yuan CZ, Zhang XG, Qian YT. Mesoporous NiO with various hierarchical nanostructures by quasi-nanotubes/nanowires/nanorods self-assembly: controllable preparation and application in supercapacitors. Cryst Eng Comm 2011;13:626–32.
[23] Ding SJ, Zhu T, Chen JS, Wang ZY, Yuan CL, Lou XW. Controlled synthesis of hierarchical NiO nanosheets hollow spheres with enhanced supercapacitive performance. J Mater Chem 2011;21:6602–6.
[24] Justin P, Meher SK, Rao GR. Tuning of capacitance behaviour of NiO using anionic, cationic, and nonionic surfactants by hydrothermal synthesis. J Phys Chem C 2010;114:5203–10.
[25] Wu MS, Wang MJ, Jow JJ. Fabrication of porous nickel oxide film with open macropores by electrophoresis and electrodepositon for electrochemical capacitors. J Power Sources 2010;195:3950–5.
[26] Vijayakumar S, Nagamuthu S, Muralidharan G. Supercapacitor studies on NiO nanoflakes synthesized through a microwave route. ACS Appl Mater Interfaces 2013;6:2188–96.
[27] Du H, Zhou C, Xie X, Li H, Qi W, Wu Y, et al. Pseudocapacitance of nanoporous Ni@NiO nanoparticles on Ni foam substrate: influence of the annealing temperature. Int J Hydrogen Energy 2017;42.22:15236–45.
[28] Kumar Ashwani, Sanger Amit, Kumar Arvind, Chandra Ramesh. Single-step growth of pyramidally textured NiO nanostructures with improved supercapacitive properties. Int J Hydrogen Energy 2017;42.9:6080–7.

[29] Tang C, Tang Z, Gong H. Highly porous Ni-Co oxide for high reversibility asymmetric fuel cell supercapacitor. J Electrochem Soc 2012;159:A651–6.
[30] Zheng Z, Huang L, Zhou Y, Hu X, Ni X. Large-scale synthesis of mesoporous CoO-doped NiO hexagonal nanoplatelets with improved electrochemical performance. Solid State Sci 2009;11:1439–43.
[31] Wu CH, Deng S, Wang H, Sun YX, Liu JB, Yan H. Preparation of novel three-dimensional NiO/ultrathin derived graphene hybrid for supercapacitor applications ACS. Appl Mater Interfaces 2014;6(2):1106–12.
[32] Zhao B, Song JS, Liu P, Xu WW, Fang T, Jiao Z, et al. Monolayer graphene/NiO nanosheets with two-dimension structure for supercapacitors. J Mater Chem 2011;21:18792–8.
[33] Ge CY, Hou ZH, He BH, Zeng FY, Cao JG, Liu YM, et al. Three dimensional flower-like nickel oxide supported on graphene sheets as an electrode material for supercapacitors. J Sol-Gel Sci Technol 2012;63:146–52.
[34] Chopra N, Claypoole L, Bachas LG. Morphological control of Ni/NiO cores/shell nanoparticles and production of hollow NiO nanostructures. J Nanopart Res 2010;12:2883–93.
[35] Kuang DB, Lei BX, Pan YP, Yu XY, Su CY. Fabrication of novel hierarchical β-$Ni(OH)_2$ and NiO microspheres via an easy hydrothermal process. J Phys Chem C 2009;113:5508–13.
[36] Ma MG, Zhu JF, Jang JX, Sun RC. Hydrothermal-polypol route to synthesis of β-$Ni(OH)_2$ and NiO in mixed solvents of 1,4-butanediol and water. Mater Lett 2009;63:1791–3.
[37] Zhang G, Yu L, Hostera HE, Wen XL. Synthesis of one-dimensional hierarchical NiO hollow nanostructures with enhanced supercapacitive performance. Nanoscale 2013;5:877–81.
[38] Xia QX, Hui KS, Hui KN, Hwang DH, Lee SK, Zhou W, et al. A facile synthesis method of hierarchically porous NiO nanosheets. Mater Lett 2012;69:69–71.
[39] Xiao J, Yang S. Bio-inspired synthesis of NaCl type $Co_xNi_{1-x}O$ ($0.025 \leq x < 0.1$) nanorods on reduced graphene oxide sheets and screening for asymmetric electrochemical capacitors. J Mater Chem 2012;22:12253–62.
[40] Purushothaman KK, Manohara Babu I, Sethuraman B, Muralidharan G. Nanosheet-assembled NiO microstructures for high-performance supercapacitors. ACS Appl Mater Interfaces 2013;5:10767–73.
[41] Xu K, Zou R, Li W, Xue Y, Song G, Liu Q, et al. Self-assembling hybrid NiO/Co_3O_4 ultrathin and mesoporus nanosheets into flower- like architectures for pseudocapacitance. J Mater Chem A 2013;1:9107–13.
[42] Sing KSW, Everett DH, Haul RAW, Moscou L, Pierotti RA, Rouquerol J, et al. Reporting physisorption data for gas/solid systems with special reference to the determination of surface area and porosity. Pure Appl Chem 1985;57:603–19.
[43] Saravanakumar B, Purushothaman KK, Muralidharan G. Interconnected V_2O_5 nanoporous network for high-performance supercapacitors. ACS Appl Mater Interfaces 2012;4:4484–90.
[44] Nagamuthu S, Vijayakumar S, Lee SH, Ryu KS. Hybrid supercapacitors based on $MnCo_2O_4$ as the positive electrode and $FeMn_2O_4$ as the negative electrode. Appl Surf Sci 2016;390:202–8.
[45] Niu L, Li Z, Sun J, Fan Z, Xu Y, Gong P, et al. Hydrothermal synthesis of Ni@C core–shell composites with high capacitance. J Alloys Compd 2013;575:152–7.
[46] Li Y, Peng H, Zhang C, Chu M, Xiao P, Zhang Y. Branched ultra-fine nickel oxide/manganese dioxide core-shell nanosheet arrays for electrochemical capacitor. RSC Adv 2015;5:77115–21.
[47] Huang M, Li F, Zhang YH, Bo Li, Gao X. Hierarchical NiO nanoflake coated CuO flower core–shell nanostructures for supercapacitor. Ceram Int 2014;40:5533–8.
[48] Liu C, Yu Z, Neff D, Zhamu A, Jang BZ. Grapheen-Based supercapacitors with an ultra high energy density. Nano Lett 2010;397:4863–8.
[49] Wang H, Wang P, Yin Z. Electrochemical capacitance of Co_xNi_yO preparation by microwave-assisted modification. Int J Electrochem Sci 2013;8:7734–43.
[50] Liu J, Jiang J, Bosman M, Fan HJ. Three-dimensional tubular arrays of MnO_2-NiO nanoflakes with high areal pseudocapacitance. J Mater Chem 2012;22:2419–26.
[51] Zang JF, Bao SJ, Li CM, Bian HJ, Cui XQ, Bao QL, et al. Well-aligned cone-shaped nanostructure of polypyrrole/RuO_2 and its electrochemical supercapacitor. J Phys Chem C 2008;112:14843–7.
[52] Park MS, Kang YM, Wang GX, Dou SX, Liu HK. The effect of morphological modification on the electrochemical properties of SnO_2 nanomaterials. Adv Funct Mater 2008;18:455–61.